Article

In-Line Monitoring of Carbon Dioxide Capture with Sodium Hydroxide in a Customized 3D-Printed Reactor without Forced Mixing

Emmanouela Leventaki [1], Francisco M. Baena-Moreno [1,*], Gaetano Sardina [2], Henrik Ström [2], Ebrahim Ghahramani [2], Shirin Naserifar [1,3], Phuoc Hoang Ho [1], Aleksandra M. Kozlowski [1] and Diana Bernin [1,*]

1   Department of Chemistry and Chemical Engineering, Chalmers University of Technology, 412 96 Gothenburg, Sweden
2   Department of Mechanical and Maritime Sciences, Chalmers University of Technology, 412 96 Gothenburg, Sweden
3   Wallenberg Wood Science Center, Chalmers University of Technology, 412 96 Gothenburg, Sweden
*   Correspondence: francisco.baena@chalmers.se (F.M.B.-M.); diana.bernin@chalmers.se (D.B.)

Abstract: Many industrial processes make use of sodium because sodium is the fifth most abundant metal and the seventh most abundant element on Earth. Consequently, there are many sodium-containing industrial wastes that could potentially be used for carbon capture, paving the way towards a circular and biobased economy. For example, a common industrial chemical is NaOH, which is found in black liquor, a by-product of the paper and pulp industry. Nonetheless, the literature available on CO_2 absorption capacity of aqueous NaOH is scarce for making a fair comparison with sodium-containing waste. Therefore, to fill this gap and set the foundation for future research on carbon capture, the CO_2 absorption capacity of NaOH solutions in a concentration range of 1–8 *w/w*% was evaluated, a wider range compared with currently available data. The data set presented here enables evaluating the performance of sodium-based wastes, which are complex mixtures and might contain other compounds that enhance or worsen their carbon capture capacity. We designed a customized reactor using a 3D-printer to facilitate in-line measurements and proper mixing between phases without the energy of stirring. The mixing performance was confirmed by computational fluid dynamics simulations. The CO_2 absorption capacity was measured via weight analysis and the progress of carbonation using a pH meter and an FTIR probe in-line. At 5 *w/w*% NaOH and higher, the reaction resulted in precipitation. The solids were analyzed with X-ray diffraction and scanning electron microscope, and nahcolite and natrite were identified. With our setup, we achieved absorption capacities in the range of 9.5 to 78.9 g CO_2/L for 1 *w/w*% and 8 *w/w*% of NaOH, respectively. The results are in fair agreement with previously reported literature, suggesting that non-forced mixing reactors function for carbon capture without the need of stirring equipment and a possible lower energy consumption.

Keywords: carbon capture and storage; aqueous bases; reactor design; chemical absorption; FTIR; absorption capacity; in-line measurements; 3D-printed reactors

1. Introduction

In recent decades, environmental changes due to increased greenhouse gas (GHG) emissions have been intensely studied [1]. Among these GHGs, it has become evident that the increased level of CO_2 in the atmosphere is one of the main contributors to these changes [2]. Consequently, interest has been growing towards developing technologies for carbon capture and storage (CCS) as a temporary but necessary solution to capture the emitted CO_2 [3,4].

Even though many different CCS technologies have been proposed to date, only a few have reached commercial status, highlighting CO_2 chemical absorption [5]. Currently, solvents such as ammonia, piperazine and amines have been proposed for their absorption of industrial CO_2 emissions, with commercial focus on the latter group [6,7]. Monoethanolamine (MEA) is one example of a commercial amine with a high capture capacity [8–10]. Despite its popularity, MEA has some significant drawbacks, such as high regeneration costs, emissions from the MEA production process, and the formation of nitrosamine—a carcinogenic compound—due to amine degradation [11,12].

Hydroxide-based solvents (i.e., NaOH or KOH) are another interesting group of solvents for CO_2 chemical absorption [11]. Indeed, NaOH has been proposed previously as an effective solvent for CO_2 capture [13–17]. Many industrial processes make use of sodium-based chemicals because sodium is the fifth most abundant metal and the seventh most abundant element on Earth. Consequently, there are many sodium-containing wastes that could potentially be used for carbon capture, paving the way towards a circular and biobased economy. The promotion of bioeconomy strategies plays a key role in the development of our society towards sustainability [18–20]. A common industrial chemical is NaOH, which is found in black liquor, a biobased residue of the paper and pulp industry [21,22]. Another example of high sodium content waste is saline industrial residue. On the other side, the regeneration of NaOH usually requires either a high energy penalty (thermal regeneration) or a chemical reaction with other compounds (chemical regeneration) [11]. Nonetheless, if NaOH comes from wastes, the carbonated solution due to CO_2 capture does not need to be regenerated. Hence, the formed carbonates could be directly stored or even used as added-value products. This is a clear example of strategies to promote bioeconomy-based and sustainable societies.

The use of an aqueous NaOH solution for CO_2 absorption has been reported in the literature [23–25]. For example, CO_2 capture from coal-fired flue gas was investigated in a continuous bubble column scrubber with efficiencies in the range of 30–98% to produce Na_2CO_3 for algae production [26]. In addition, parameters such as absorption efficiency and mass-transfer coefficient were evaluated [26]. A comparison of removal efficiencies of CO_2 between aqueous ammonia and an aqueous NaOH solution in a fine spray column was carried out [27]. These authors targeted a CO_2 removal efficiency of 90% and reported the corresponding mole ratios of solvent to CO_2 to be 4.43 and 9.68 for NaOH and aqueous ammonia, respectively. These findings further suggest the advantages of NaOH for CO_2 capture over other solvents. Another very interesting study proposed capturing CO_2 from air by spraying NaOH. The expenses of this CO_2 capturing alternative ranged from 53 to 127 \$/ton CO_2 [28]. Aqueous NaOH was also used to capture CO_2 in a two-stage combined process, in which $Ca(OH)_2$ was utilized to obtain $CaCO_3$ and regenerate the NaOH. The authors obtained CO_2 absorption efficiencies of 67.85% and regeneration rates for NaOH of 85.37% [29]. As summarized, the use of NaOH for CO_2 capture has been studied.

Nonetheless and despite the importance of aqueous NaOH solutions for CO_2 capture with sodium-based wastes and to the best of our knowledge, only one work has dealt with the estimation of absorption capacities of CO_2 in aqueous NaOH solutions. This is crucial to estimate the performance of other sodium-based wastes and to validate the performance of alternative reactor designs. Yoo Miran et al. evaluated the absorption capacity of a gas stream containing 30 *v/v*% CO_2 for different concentrations of aqueous NaOH solutions (1–5 *w/w*%) [17]. In this work, authors measured the absorption capacity through a combination of experiments i.e., the CO_2 concentration in the outcoming gas stream, the pH value and the electrical conductivity of the solution over time. Furthermore, they predicted the evolution of chemical species in the solutions with time. However, for a mechanistic optimization of future carbonation reactors, it is crucial to monitor the chemical reactions occurring during absorption. Furthermore, it is necessary to expand the studied concentration range to values typically found in waste solutions [21,22]. Hence, to fulfill these knowledge gaps, the present study measured the absorption of CO_2 in aqueous solutions of NaOH up to 8 *w/w*% at ambient pressure and temperature. Importantly, the

absorption was monitored using an analytical balance and the progress of the chemical reactions inside the reactor was followed with a pH meter and an FTIR probe. We observed the formation of carbonate and bicarbonate ions and absorption of CO_2 depending on pH. This opens new avenues for optimization either for maximum absorption capacity or the formation of value-added products.

In addition, we customized the reactor design for non-forced mixing, which reduces the amount of equipment and possibly the amount of energy needed. The reactor enabled also in-line measurements and was 3D printed using a resin printer. Its mixing performance was corroborated by computational fluid dynamics (CFD) simulations. All experiments were conducted in this customized 3D-printed bubble batch reactor using bubble motion to create mixing.

At solutions of 5 *w/w*% NaOH and higher, solid carbonate and bicarbonate species were formed due to saturation. The solids were analyzed with X-ray diffraction and scanning electron microscopy and natrite (Na_2CO_3) and nahcolite ($NaHCO_3$) were identified. With our setup, we achieved absorption capacities in the range of 9.5 to 78.9 g CO_2/L for 1 *w/w*% and 8 *w/w*% of NaOH, respectively. The results are in fair agreement with previously reported literature findings that non-forced mixing reactors function for carbon capture and may entail economic advantages compared to stirring-based ones. This assessment is however out of the scope of this study. With this work, we aimed to lay the foundation for future works for sustainable CO_2 capture using wastes with a high sodium content. Furthermore, the results enable finding suitable conditions for reaching either a high absorption rate, a maximum absorption capacity or value-added species formed by absorption.

2. Materials and Methods

2.1. Materials

Aqueous NaOH solutions were prepared by dissolving high purity NaOH (VWR, 99% purity) in distilled water to give concentrations ranging from 1–8 *w/w*%. The gas mixture had a composition of 30 *v/v*% CO_2 and 70 *v/v*% N_2. This composition has been previously used by other authors [17]. A stereolithography (SLA) 3D-printer Form 3+ (Formlabs) was used to print a custom designed reactor of the UV curable resin Rigid 10K (Formlabs). The reactor was designed using the CAD software Autodesk Fusion 360.

2.2. Experimental Setup, Procedures, and Reactor Design

Figure 1 shows the experimental setup used for CO_2 carbonation experiments. The gas mixture of CO_2 and N_2 was flowing at a steady rate of 200 mL/min adjusted with a pressure regulator and monitored with an in-line flowmeter. The gas passed through a sparger into the 3D-printed reactor, which was filled with 60 mL solution. For each NaOH concentration, experiments were carried out using two different setups. The first setup included the pH-meter (HQ430D, HACH, Loveland, CO, USA) and the FTIR (ReactIR 702L, Mettler Toledo, Greifensee, Switzerland) probe immersed in the solution to record pH and FTIR spectra with time (Figure 1A). The experiments were stopped once the pH reached a value of 8 because below this threshold the amount of absorbed CO_2 is insignificant. To measure the absorption capacity, a second experiment was performed for the same duration as the first with the 3D-printed reactor mounted on a balance (QUINTIX2102-1S, Sartorius, Göttingen, Germany), which was connected to a computer for data logging (Figure 1B). The pH value was checked at the end of this second run to corroborate that an identical pH value was reached.
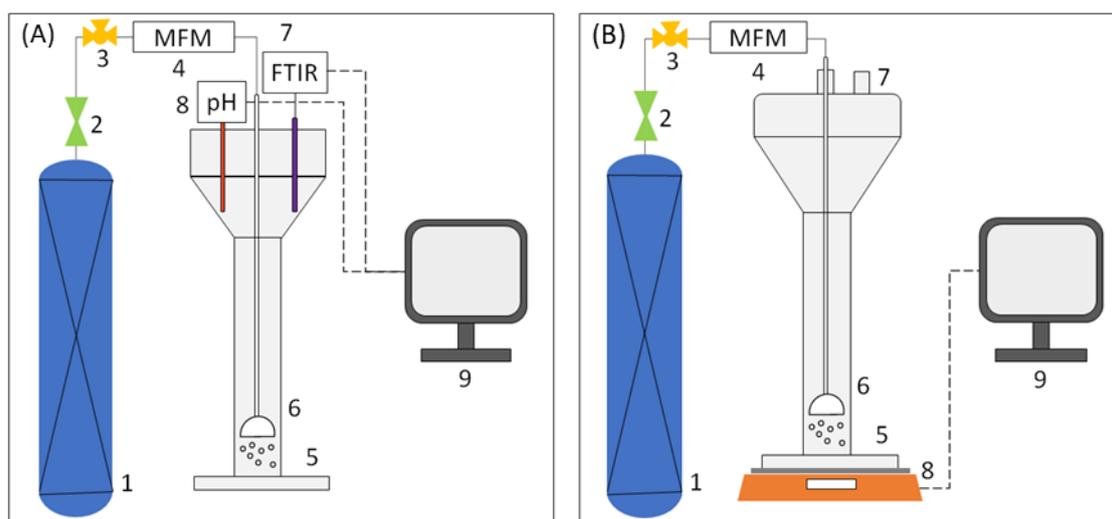
Figure 1. Experimental setups: (**A**) The first run includes 1. gas bottle (30 *v/v*% CO_2, 70 *v/v*% N_2), 2. pressure regulator, 3. three-way valve, 4. mass flow meter, 5. reactor, 6. sparger, 7. FTIR, 8. pH-meter, 9. computer for data logging; (**B**) The second run includes 1. gas bottle (30 *v/v*% CO_2, 70 *v/v*% N_2), 2. pressure regulator, 3. three-way valve, 4. mass flow meter, 5. reactor, 6. sparger, 7. gas outlet, 8. balance, 9. computer for data logging.

The FTIR spectrum of air was subtracted as background from the obtained FTIR spectra prior to analysis. For 5 *w/w*% NaOH and higher, precipitation occurred. The formed solid product was filtered and dried prior to X-ray Diffraction (XRD) and Scanning Electron Microscope (SEM) characterization. X-ray diffraction (XRD) measurements were performed on the D8 Discover Bruker instrument. The patterns were recorded for a diffraction angle range of 2θ from 10 to 70° with a scan step of 0.02° per second. The peaks of the obtained phases were matched with peaks present in the database (PDF-4-2021) from the International Centre for Diffraction Data (ICDD). SEM images were obtained using a Phenom ProX Desktop SEM (ThermoFisher Scientific, Waltham, MA, USA).

Concerning the reactor design, there are two important processes during optimized gas absorption, (1) enhancing the mass transfer of the gas into the liquid through the bubble surface and (2) avoiding saturation of the absorbed gas in the liquid phase in the reactor. Raising bubbles introduce a fluid motion upwards followed by a down-coming fluid motion elsewhere by continuity. However, these upwards and downwards flows depend on the size of the reactor cross-section. The reactor was designed to have a narrow and long body with the gas sparged from the bottom enabling homogenous mixing caused by the bubble motion without the need for forced mixing. This reduces the need of additional equipment and energy for stirring. The 3D-printed reactor design and its dimensions can be seen in Figure 2.

The top of the vessel is wider to allow the pH meter and FTIR probe to be immersed in the solution. The non-absorbed gas escaped to the atmosphere through the gas outlet and could have carried a small amount of solution resulting in a loss of weight. Evaporation of the solvent also occurred during absorption. Hence, blank experiments were carried out to evaluate the losses. These experiments were conducted by sparging the same gas mixture through distilled water, with the reactor mounted on the analytical balance and measuring the weight loss with time. The obtained weight loss trend from the blank runs was included in the data treatment to compensate for the solvent losses.
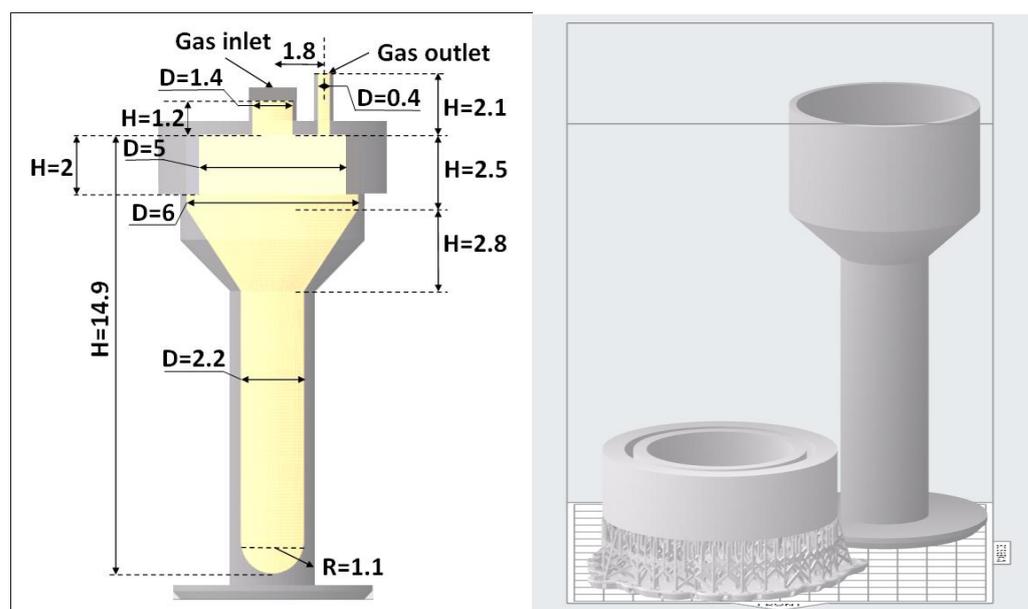
Figure 2. Dimensions (**left**) and design of reactor in Autodesk Fusion 360 (**right**).

*2.3. Computational Fluid Dynamics (CFD) Methodology*

To qualitatively address the flow field inside the reactor geometry and evaluate the degree of mixing of the solution, we employed CFD using an unstructured mesh of 11,428 cells to solve the non-reactive multiphase model equations in the reactor. We employed a two-fluid Eulerian-Eulerian model to describe the suspension of CO_2 and N_2 bubbles in water. In particular, the CO_2 and N_2 components are treated as a gas phase while the water is the liquid phase. Gas and liquid volume fractions measure the relative concentration of the two components in each part of the reactor. Following the experimental procedure, the gas phase is injected into the domain from the sparger after starting to rise along the liquid phase driven by buoyancy effects. Turbulence in the liquid phase was modeled using a modified version of the k-ε model, adapted for turbulent bubbly suspensions [30]. The momentum exchange term between the two-phases includes drag, lift and virtual mass forces, moreover, turbulent dispersion was also included using the Favre-averaged drag relationship developed in [31].

We used the software ANSYS Fluent R2021 V2 for our simulations. The temporal discretization is first-order implicit with a time step of 10^{-4} s, the pressure-velocity coupling is handled by the Phase Coupled scheme SIMPLE, and the pressure interpolation is body force weighted. Convective terms and volume fractions are discretized using the QUICK scheme while the turbulent equations employ a first-order upwind in the non-linear terms.

3. Theoretical Considerations of Carbonation Reactions of CO_2 in Aqueous Bases

For a comprehensive explanation of the theory involved in carbonation reactions, readers are referred to reference [17]. In this section, the essentials of carbonation reactions of CO_2 in aqueous bases are described. As the system has two phases, liquid and gas, the process is dictated by two phenomena, the physical transition of CO_2 from the gas bubble to the liquid, and the chemical reaction between the absorbed CO_2 and the OH^-. The following three different forms, the carbonate ion CO_3^{2-}, the bicarbonate ion HCO_3^- and carbonic acid H_2CO_3, exist in an aqueous solution depending on the pH [32].

At pH above 12.3, CO_2 reacts with OH^- ions to form CO_3^{2-} ions according to Equation (1).

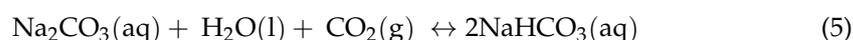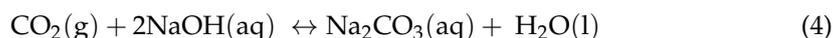$$CO_2 + 2OH^- \leftrightarrow CO_3^{2-} + H_2O \tag{1}$$
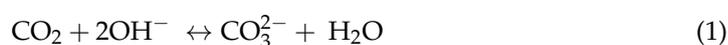
As the OH^- ions are consumed i.e., the pH is lowered, the CO_2 converts to both carbonate and bicarbonate ions. The two species exist in equilibrium dependent on pH and below a specific pH only bicarbonate ions are formed according to Equation (2).

$$CO_2 + OH^- \leftrightarrow HCO_3^- \tag{2}$$

Finally, at pH = 4.3 and lower, all of the CO_2 turns into carbonic acid (Equation (3)).

$$CO_2 + H_2O \leftrightarrow H_2CO_3 \tag{3}$$

The carbonation of CO_2 with NaOH occurs in two steps to form sodium carbonate (Equation (4)) and bicarbonate (Equation (5)) [15].

$$CO_2(g) + 2NaOH(aq) \leftrightarrow Na_2CO_3(aq) + H_2O(l) \tag{4}$$

$$Na_2CO_3(aq) + H_2O(l) + CO_2(g) \leftrightarrow 2NaHCO_3(aq) \tag{5}$$

Sodium carbonate and bicarbonate have a high solubility in water up to 30.7 g/100 g water and 10.3 g/100 g water respectively at room temperature [33]. In contrast, carbonic acid has very low solubility i.e., once the pH drops to favor the production of carbonic acid, the absorption of CO_2 is reduced significantly [34].

4. Results

4.1. Mixing in the Reactor

The first step is to corroborate that the reactor shape allows suitable mixing, which was confirmed in CFD simulations. Figure 3 shows the flow fields computed using the CFD numerical approach. Panel (A) represents the gas volume fraction inside the reactor along a vertical section. The gas bubbly phase is injected from the sparger, close to the bottom of the reactor. The highest relative concentration is found near the injection point, as indicated by the red-orange color. Afterwards, the gas rises along the vertical axis, decreasing the relative concentration compared to the liquid phase (represented by green and blue colors). The order of magnitude of the gas velocities inside the reactor can be seen in panel (B) of Figure 3, where the highest velocity of around 0.3 m/s is found close to the inner wall of the reactor immediately on top of the sparger. Finally, to evaluate the degree of mixing of the gas phase inside the reactor, we compare the ratio between the turbulent viscosity and molecular viscosity of the suspension (Panel C).

Since the reactor does not have rotating stirring parts, turbulence is needed to reach a good mixing because molecular diffusion is too slow. The regions inside the reactor with a high ratio between turbulent and molecular viscosity will give an indication of the preferential zones where mixing is achieved. From Figure 3C, it can be observed that the lower part of the reactor, on top of the sparger, is characterized by a turbulent viscosity ratio that is up to one order of magnitude the molecular viscosity of the water, suggesting that this is the region with the highest degree of mixing inside the reactor. The good level of mixing is confirmed by looking at the gas volume fraction distribution in Figure 3A where, after the mixing region, a uniform gas concentration in the horizontal plane is achieved at around 50% of the volume fraction (green contour). Overall, these results confirm that the reactor design is adequate: the bubble motion creates a suitable mixing environment without the need for any additional power input by stirring.
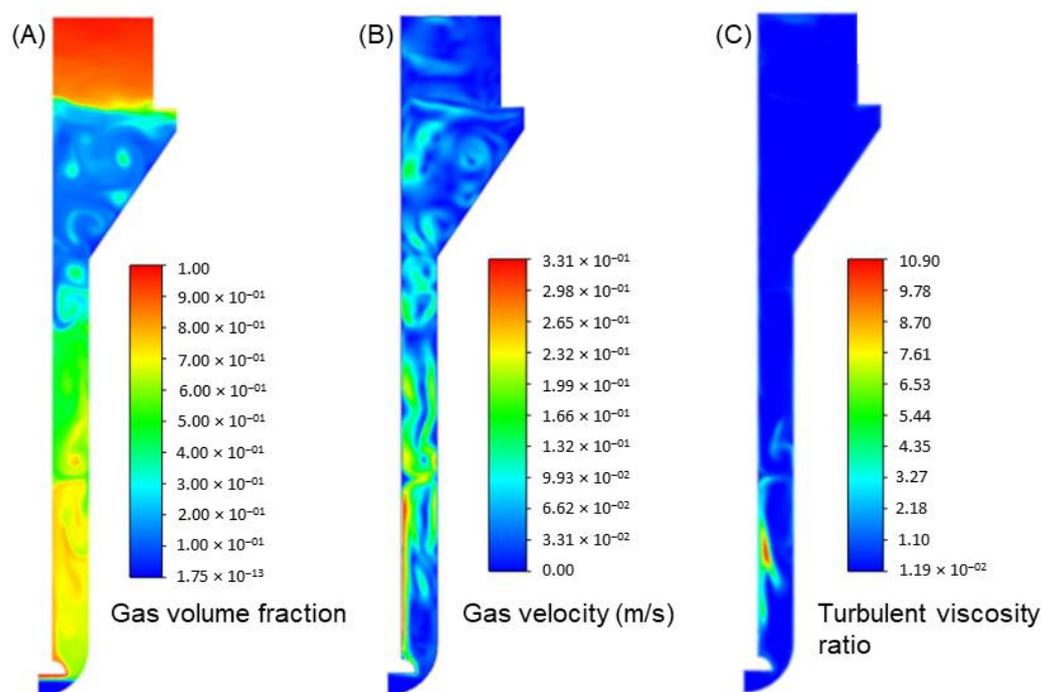
Figure 3. Contour plots of the gas volume fraction (**A**), gas velocity (**B**) and turbulent viscosity ratio (**C**) obtained from the CFD simulations.

4.2. Carbonation Reactions and Reactor Performance

The FTIR probe provided insights for understanding the occurring chemical reactions over time. Carbonate ions appear with a strong peak at around 1380 cm^{-1}, bicarbonate ions with a lower intensity at around 1360 cm^{-1}, 1300 cm^{-1} and 1008 cm^{-1} and water at around 1635 cm^{-1}, as highlighted in Figure 4E [35]. Unfortunately, the bicarbonate ion peaks at 1360 cm^{-1} and 1300 cm^{-1} overlap with the carbonate ion peak, which complicates quantification of each species. FTIR spectra as a function of wavenumber and time of all NaOH solutions are shown in Figure 4. The carbonate ion peak appears from 2 *w/w*% (B) while the bicarbonate ion peak starts to be visible from 3 *w/w*% (C). Furthermore, the carbonate ion peak grows first with time before a shift to lower wavenumbers is observed. This is true for all samples.

It is noteworthy that the intensities of the carbonate ion peaks in comparison with the water peak increased up to a NaOH concentration of 6 *w/w*% (F). For example, 2 *w/w*% NaOH (A), the carbonate ion peak at 1380 cm^{-1} is only slightly noticeable in contrast to 4 *w/w*% NaOH (D) revealing strong carbonate and bicarbonate ion peaks. This might indicate that the intensity of the observed carbonate ion peaks albeit overlapping signals may be correlated with its amount not only with time but also between samples. This observation might provide insights for CO_2 absorption in sodium-based wastes. At 5 *w/w*% NaOH and higher, precipitation occurred. This might be attributed to a stagnation of the intensity increase of the carbonate ion peak compared with the water peak. In the case of the 8 *w/w*% NaOH, the pattern of the FTIR spectra changed, which might be initiated by precipitation. Due to the gas bubbling, most of the solid particles were most likely dispersed in the reactor causing an interference of the FTIR measurement.

The formed solids that precipitated for the 6 *w/w*% were analyzed with XRD and SEM. The obtained SEM images presented in Figure 5A–D reveal irregular, rectangular and needle shapes. The obtained XRD pattern corresponds to a mix of natrite (main peaks at 26°, 27.5°, 33°, 35°, 38°, 40°, 41.5°, 46.5°, 47°, 48°, and all the other peaks from 53.5°), and to a minor extend of nahcolite (main peaks at 30°, 34.5°, and 44.5°) as shown in Figure 5E. Similar shapes and crystal structures were also found in previous works both from an after-process product [36] and commercial $NaHCO_3$ production before utilization [37].
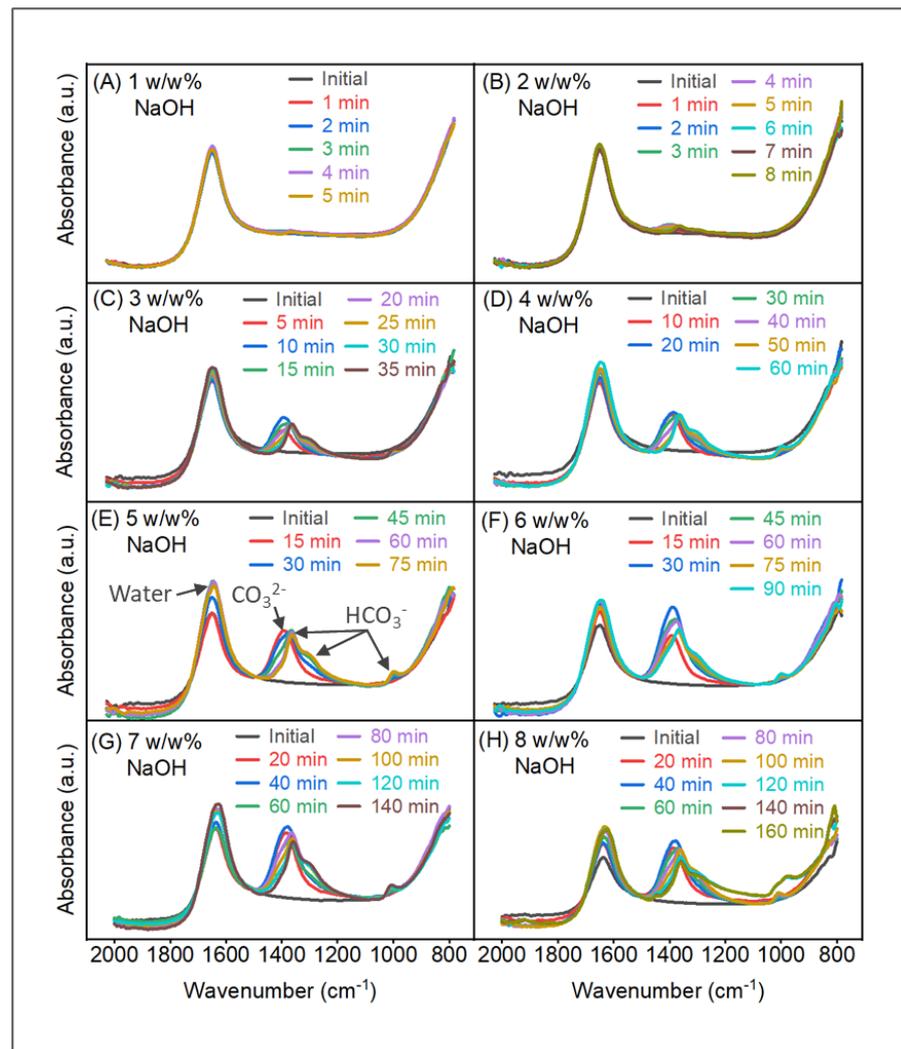
Figure 4. FTIR spectra of CO_2 absorption in NaOH solutions with time for (**A**) 1 *w/w%*; (**B**) 2 *w/w%*; (**C**) 3 *w/w%*; (**D**) 4 *w/w%*; (**E**) 5 *w/w%*; (**F**) 6 *w/w%*; (**G**) 7 *w/w%*; (**H**) 8 *w/w%*.
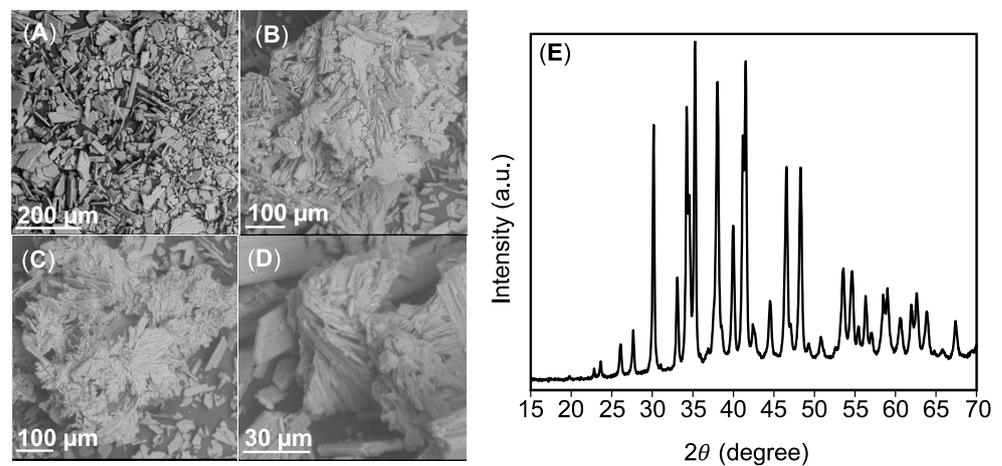

Figure 5. SEM images (**A**–**D**) and XRD diffractogram (**E**) of the powder obtained for 6 *w/w%* NaOH.

The CO_2 carbonation and absorption of the NaOH solutions were successfully monitored using an analytical balance, pH meter and FTIR probe. The increase in weight with time corresponded directly to the captured amount of CO_2. The pH and FTIR data agreed with the results of the balance and provided insight into the chemical reactions occurring

during the absorption, as explained in Section 4.2. The pH value prior to absorption is 12.4 for the 1 *w/w*% NaOH solutions and 13.5 for the 8 *w/w*%. It decreased upon the consumption of OH^- ions due to the formation of carbonate and bicarbonate ions. This formation could be followed by FTIR as explained in Section 4.2 (see typical FTIR spectrum in Figure 4E). Hence, the sum of absorbance values in the regions 1372–1388 cm^{-1} for the carbonate ion and 1000–1016 cm^{-1} for the bicarbonate ion were plotted with time to reflect their formation during absorption.

Figure 6 shows an example of all measurements obtained with time for 4 *w/w*% NaOH providing a clear picture of the progress of absorption. In the beginning the absorption rate of CO_2 was high and all absorbed CO_2 was converted into carbonate ions (A). The highest absorption rate occurred within the first 6 min until a pH value of 12.9. Up to that point, the CO_2 absorption was 12.4 g/L. After approximately 11 min, the pH dropped from 12.3 to 10.2 with the highest drop rate at pH 11.2 (B). At the same point in time, according to the sum of absorbance intensities (C), the formation of carbonate ions reached a maximum, and bicarbonate ions started to emerge (D). The absorption of CO_2 up to that point was 19.8 g/L. After 24.5 min, the pH continued dropping at a much slower rate and it took 35 additional minutes to decrease from 9.6 to 8.0 (B). During that time, 11.5 g/L of CO_2 was absorbed until the experiment was stopped at pH 8. These absorption trends were previously reported by [17], which confirms that the proposed reactor design produces the same results as forced-mixing reactors. Nevertheless, our results including FTIR verified that the formation of carbonate and bicarbonate ions depends on pH and absorption capacity. This wealth of data enables optimizing the duration of the reaction to maximum absorption rate or capacity or value-added products.
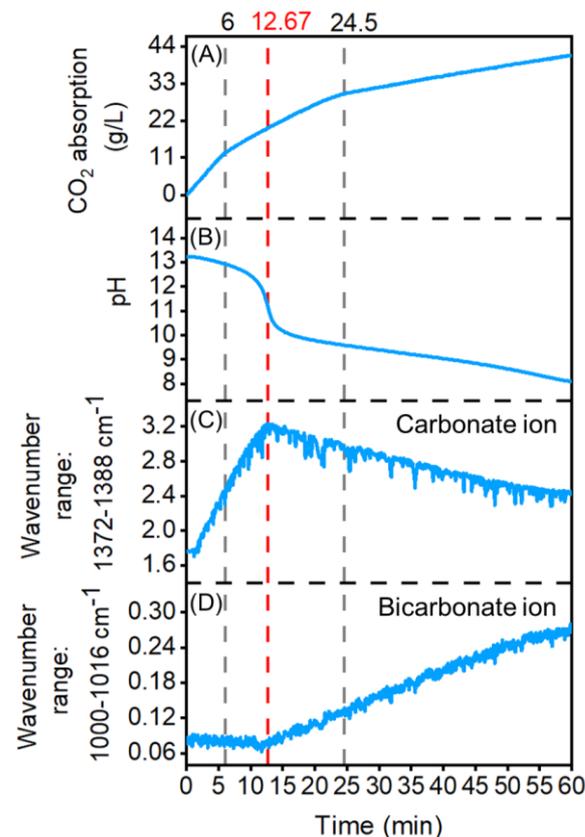

Figure 6. CO_2 absorption (**A**), pH (**B**), the sum of the absorbance intensities of the wavenumber range 1372–1388 cm^{-1} corresponding to the carbonate ion region (**C**) and the sum of the absorbance intensity of the wavenumber range 1000–1016 cm^{-1} corresponding to the bicarbonate ion region (**D**) with time for 4 *w/w*% NaOH.

Solutions of 1 to 8 *w/w*% NaOH were prepared to obtain a mechanistic understanding of the concentration-absorption rate dependence. The increase in weight with time due to CO_2 absorption of three solutions of 1, 4 and 8 *w/w*% NaOH is shown in Figure 7. The total duration of the experiments to reach pH 8 became longer with increasing NaOH concentration. For the 1 *w/w*% NaOH solution, it took 4.5 min (A) while for the 8 *w/w*% it lasted 2 h and 20 min (C). Furthermore, for the 1 *w/w*% NaOH, the rate of absorption was relatively constant throughout the experiment in contrast to the 4 and 8 *w/w*% NaOH solutions for which the rate levelled out with time. Interestingly, the same amount of CO_2 absorption for the 4 *w/w*%, 40 g/L, was reached after roughly 1/3 of the duration for 8 *w/w*% NaOH. This finding suggests that the amount of OH^- ions present in solution i.e., pH, is the driving force for the absorption rate. Below pH 8, CO_2 is still being absorbed at a very low rate until complete saturation and the weight stabilizes. These experiments were not run until rate depletion because such a low rate is not of interest from an industrial perspective.
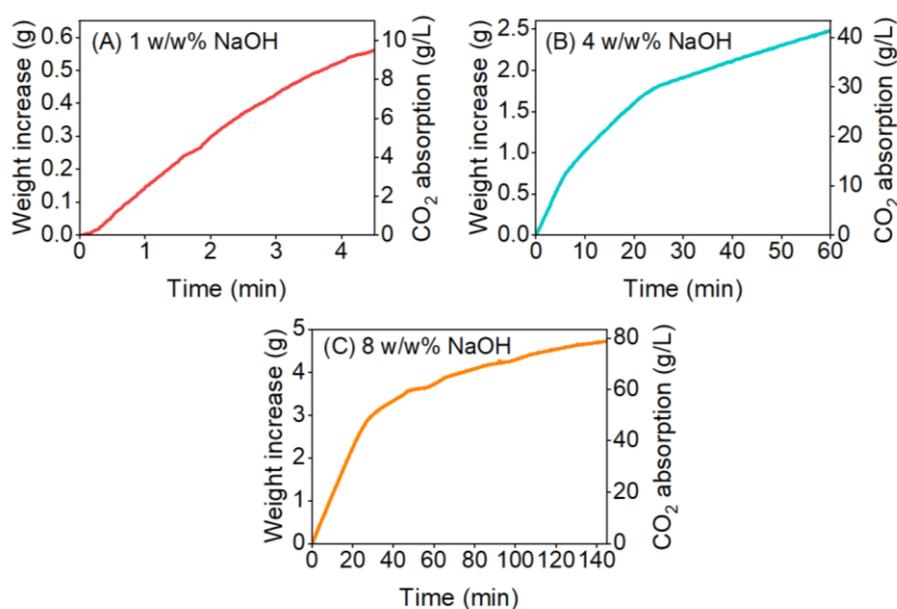

Figure 7. Weight increase of the reactor and the corresponding CO_2 absorption for 1 (**A**), 4 (**B**) and 8 (**C**) *w/w*% NaOH.

Figure 8A compares the experimental absorption capacities with the theoretical values if all CO_2 reacts forming carbonate and bicarbonate ions, respectively. These theoretical absorption capacities were calculated as the stoichiometric amount of CO_2 that reacts completely towards carbonates or bicarbonates according to Equations (1) and (2). This can only be used as a guideline because for most of the studied pH range here, carbonate and bicarbonate ions will form. The absorption capacities are between the two theoretical values, indicating that a mixture of carbonate and bicarbonate ions was produced at the end of the reaction. This agrees with the chemical reactions occurring at this pH (Equations (1) and (2)) and has also been verified by the FTIR spectra as we will explain in the next section. Additionally, it appeared that the absorption capacity has an almost linear correlation with the concentration of NaOH as shown in Figure 8B. This correlation and the absorption capacities for 1–5 *w/w*% NaOH agreed well with the trends and values reported in the literature [17]. This further proves that the 3D-printed reactor without forced mixing produces the same absorption capacities as those reactors employing forced mixing. Consequently, the presented solution has a clear advantage from an energy consumption perspective.
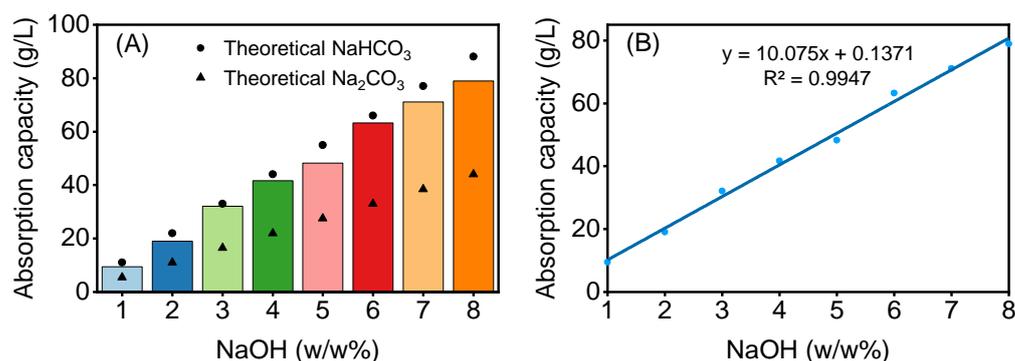
Figure 8. (**A**) Obtained and theoretical absorption capacities for NaOH solutions of 1 to 8 *w/w*% NaOH. A total conversion of CO_2 to carbonate and bicarbonate ions was assumed to estimate the theoretical capacities using Equations (1) and (2). (**B**) Linear regression based on the experimental data, indicating that the concentration of NaOH and the absorption capacity correlate linearly.

5. Conclusions and Future Remarks

Herein the absorption capacity of aqueous NaOH solutions for CO_2 capture was assessed for a wide range of concentrations (1–8 *w/w*%) with a 3D-printed reactor that avoids forced-mixing. The experimental setup included an in-line FTIR probe and pH meter to monitor the reaction over time and an analytical balance to estimate the absorption capacity through weight increase. Overall, the obtained CO_2 absorption capacities were in the range of 9.5 to 78.9 g/L for 1 *w/w*% and 8 *w/w*%, respectively. Reported capacities and crystal structures agreed with our results confirming that the non-forced mixing reactor design functions for CO_2 capture, which is an advantage from an energy and equipment savings perspective. Furthermore, monitoring the formation of carbonate and bicarbonate ions concurrently with pH and CO_2 absorption paves the way for optimizing the duration of the reaction for the maximum absorption rate or capacity or value-added products. The further optimization of absorption rate can be performed by adjusting the NaOH concentration. The 3D-printed design allows for easy implementation and hence applications for sodium-based wastes. The absorption capacity of such wastes can now be compared to aqueous NaOH solutions and optimized for different purposes and processes, such as the use of industrial waste to promote circularity in our societies. There are many sodium-containing industrial waste and its use for carbon capture undoubtedly boost the transition towards a biobased economy.

Author Contributions: Conceptualization, E.L., F.M.B.-M. and D.B.; methodology, E.L., F.M.B.-M., G.S. and H.S.; software, G.S., H.S. and E.G.; validation, F.M.B.-M. and D.B.; formal analysis, E.L., F.M.B.-M. and D.B.; investigation, E.L., F.M.B.-M., G.S., H.S. and D.B.; resources, G.S., H.S. and D.B.; data curation, E.L., F.M.B.-M., S.N., P.H.H. and A.M.K.; writing—original draft preparation, E.L., F.M.B.-M., G.S. and D.B.; writing—review and editing, E.L., F.M.B.-M. and D.B.; visualization, E.L., F.M.B.-M. and D.B.; supervision, G.S., H.S. and D.B.; project administration, G.S., H.S. and D.B.; funding acquisition, G.S., H.S. and D.B.. All authors have read and agreed to the published version of the manuscript.

Institutional Review Board Statement: Not applicable.

Informed Consent Statement: Not applicable.

Data Availability Statement: Not applicable.

Conflicts of Interest: The authors declare no conflict of interest.

References

1. Ritchie, H.; Roser, M.; Rosado, P. CO$_2$ and Greenhouse Gas Emissions. Available online: https://ourworldindata.org/co2-and-other-greenhouse-gas-emissions (accessed on 18 July 2022).
2. Witte, K. Social Acceptance of Carbon Capture and Storage (CCS) from Industrial Applications. *Sustainability* **2021**, *13*, 12278. [CrossRef]
3. Fichera, A.; Samanta, S.; Volpe, R. Exergetic Analysis of a Natural Gas Combined-Cycle Power Plant with a Molten Carbonate Fuel Cell for Carbon Capture. *Sustainability* **2022**, *14*, 533. [CrossRef]
4. Kheirinik, M.; Ahmed, S.; Rahmanian, N. Comparative Techno-Economic Analysis of Carbon Capture Processes: Pre-Combustion, Post-Combustion, and Oxy-Fuel Combustion Operations. *Sustainability* **2021**, *13*, 13567. [CrossRef]
5. Vega, F.; Baena-Moreno, F.M.; Gallego Fernández, L.M.; Portillo, E.; Navarrete, B.; Zhang, Z. Current Status of CO$_2$ Chemical Absorption Research Applied to CCS: Towards Full Deployment at Industrial Scale. *Appl. Energy* **2020**, *260*, 114313. [CrossRef]
6. Mohd Pauzi, M.M.; Azmi, N.; Lau, K.K. Emerging Solvent Regeneration Technologies for CO$_2$ Capture through Offshore Natural Gas Purification Processes. *Sustainability* **2022**, *14*, 4350. [CrossRef]
7. Sánchez-Bautista, A.; Palmero, E.M.; Moya, A.J.; Gómez-Díaz, D.; la Rubia, M.D. Characterization of Alkanolamine Blends for Carbon Dioxide Absorption. Corrosion and Regeneration Studies. *Sustainability* **2021**, *13*, 4011. [CrossRef]
8. Ji, L.; Yu, H.; Li, K.; Yu, B.; Grigore, M.; Yang, Q.; Wang, X.; Chen, Z.; Zeng, M.; Zhao, S. Integrated Absorption-Mineralisation for Low-Energy CO$_2$ Capture and Sequestration. *Appl. Energy* **2018**, *225*, 356–366. [CrossRef]
9. Hong, S.; Sim, G.; Moon, S.; Park, Y. Low-Temperature Regeneration of Amines Integrated with Production of Structure-Controlled Calcium Carbonates for Combined CO$_2$ Capture and Utilization. *Energy Fuels* **2020**, *34*, 3532–3539. [CrossRef]
10. Arti, M.; Youn, M.H.; Park, K.T.; Kim, H.J.; Kim, Y.E.; Jeong, S.K. Single Process for CO$_2$ Capture and Mineralization in Various Alkanolamines Using Calcium Chloride. *Energy Fuels* **2017**, *31*, 763–769. [CrossRef]
11. Baena-Moreno, F.M.; Rodríguez-Galán, M.; Vega, F.; Ramirez-Reina, T.; Vilches, L.; Navarrete, B. Understanding the Influence of the Alkaline Cation K $^+$ or Na $^+$ in the Regeneration Efficiency of a Biogas Upgrading Unit. *Int. J. Energy Res.* **2019**, *43*, 1578–1585. [CrossRef]
12. Luis, P. Use of Monoethanolamine (MEA) for CO$_2$ Capture in a Global Scenario: Consequences and Alternatives. *Desalination* **2016**, *380*, 93–99. [CrossRef]
13. Mahmoudkhani, M.; Keith, D.W. Low-Energy Sodium Hydroxide Recovery for CO$_2$ Capture from Atmospheric Air—Thermodynamic Analysis. *Int. J. Greenh. Gas Control.* **2009**, *3*, 376–384. [CrossRef]
14. Hikita, H.; Asai, S.; Takatsuka, T. Absorption of Carbon Dioxide into Aqueous Sodium Hydroxide and Sodium Carbonate-Bicarbonate Solutions. *Chem. Eng. J.* **1976**, *11*, 131–141. [CrossRef]
15. Shim, J.-G.; Lee, D.W.; Lee, J.H.; Kwak, N.-S. Experimental Study on Capture of Carbon Dioxide and Production of Sodium Bicarbonate from Sodium Hydroxide. *Environ. Eng. Res.* **2016**, *21*, 297–303. [CrossRef]
16. Lucile, F.; Cézac, P.; Contamine, F.; Serin, J.-P.; Houssin, D.; Arpentinier, P. Solubility of Carbon Dioxide in Water and Aqueous Solution Containing Sodium Hydroxide at Temperatures from (293.15 to 393.15) K and Pressure up to 5 MPa: Experimental Measurements. *J. Chem. Eng. Data* **2012**, *57*, 784–789. [CrossRef]
17. Yoo, M.; Han, S.-J.; Wee, J.-H. Carbon Dioxide Capture Capacity of Sodium Hydroxide Aqueous Solution. *J. Environ. Manag.* **2013**, *114*, 512–519. [CrossRef]
18. D'Adamo, I.; Gastaldi, M.; Morone, P.; Rosa, P.; Sassanelli, C.; Settembre-Blundo, D.; Shen, Y. Bioeconomy of Sustainability: Drivers, Opportunities and Policy Implications. *Sustainability* **2021**, *14*, 200. [CrossRef]
19. D'Adamo, I.; Sassanelli, C. Biomethane Community: A Research Agenda towards Sustainability. *Sustainability* **2022**, *14*, 4735. [CrossRef]
20. D'Adamo, I.; Gastaldi, M. Sustainable Development Goals: A Regional Overview Based on Multi-Criteria Decision Analysis. *Sustainability* **2022**, *14*, 9779. [CrossRef]
21. Cardoso, M.; de Oliveira, É.D.; Passos, M.L. Chemical Composition and Physical Properties of Black Liquors and Their Effects on Liquor Recovery Operation in Brazilian Pulp Mills. *Fuel* **2009**, *88*, 756–763. [CrossRef]
22. Reyes, L.; Nikitine, C.; Vilcocq, L.; Fongarland, P. Green Is the New Black—A Review of Technologies for Carboxylic Acid Recovery from Black Liquor. *Green Chem.* **2020**, *22*, 8097–8115. [CrossRef]
23. Kordylewski, W.; Sawicka, D.; Falkowski, T. Laboratory Tests on the Efficiency of Carbon Dioxide Capture from Gases in Naoh Solutions. *J. Ecol. Eng.* **2013**, *14*, 54–62. [CrossRef]
24. Salmón, I.; Cambier, N.; Luis, P. CO$_2$ Capture by Alkaline Solution for Carbonate Production: A Comparison between a Packed Column and a Membrane Contactor. *Appl. Sci.* **2018**, *8*, 996. [CrossRef]
25. Azizi, F.; Kaady, L.; Al-Hindi, M. Chemical Absorption of CO$_2$ in Alkaline Solutions Using an Intensified Reactor. *Can. J. Chem. Eng.* **2022**, *100*, 2172–2190. [CrossRef]
26. Chen, P.C.; Huang, C.F.; Chen, H.-W.; Yang, M.-W.; Tsao, C.-M. Capture of CO$_2$ from Coal-Fired Power Plant with NaOH Solution in a Continuous Pilot-Scale Bubble-Column Scrubber. *Energy Procedia* **2014**, *61*, 1660–1664. [CrossRef]
27. Yincheng, G.; Zhenqi, N.; Wenyi, L. Comparison of Removal Efficiencies of Carbon Dioxide between Aqueous Ammonia and NaOH Solution in a Fine Spray Column. *Energy Procedia* **2011**, *4*, 512–518. [CrossRef]
28. Stolaroff, J.K.; Keith, D.W.; Lowry, G.V. Carbon Dioxide Capture from Atmospheric Air Using Sodium Hydroxide Spray. *Environ. Sci. Technol.* **2008**, *42*, 2728–2735. [CrossRef]

29. Zhou, P.; Wang, H. Carbon Capture and Storage—Solidification and Storage of Carbon Dioxide Captured on Ships. *Ocean. Eng.* **2014**, *91*, 172–180. [CrossRef]

30. Pfleger, D.; Becker, S. Modelling and Simulation of the Dynamic Flow Behaviour in a Bubble Column. *Chem. Eng. Sci.* **2001**, *56*, 1737–1747. [CrossRef]

31. Burns, A.D.; Frank, T.; Hamill, I.; Shi, J.M. The Favre Averaged Drag Model for Turbulent Dispersion in Eulerian Multi-Phase Flows. In Proceedings of the Fifth International Conference on Multiphase Flow, Yokohama, Japan, 30 May–4 June 2004.

32. Wolf-Gladrow, D.A.; Zeebe, R.E.; Klaas, C.; Körtzinger, A.; Dickson, A.G. Total Alkalinity: The Explicit Conservative Expression and Its Application to Biogeochemical Processes. *Mar. Chem.* **2007**, *106*, 287–300. [CrossRef]

33. *CRC Handbook of Chemistry and Physics*; Haynes, W.M. (Ed.) CRC Press: Boca Raton, FL, USA, 2014; ISBN 9780429170195.

34. Wishart, D.S.; Guo, A.; Oler, E.; Wang, F.; Anjum, A.; Peters, H.; Dizon, R.; Sayeeda, Z.; Tian, S.; Lee, B.L.; et al. HMDB 5.0: The Human Metabolome Database for 2022. *Nucleic Acids Res.* **2022**, *50*, D622–D631. [CrossRef]

35. National Institute of Standards and Technology NIST Chemistry WebBook. Available online: http://webbook.nist.gov (accessed on 18 July 2022).

36. Salvador Cob, S. *Towards Zero Liquid Discharge in Drinking Water Production*; TU Delft: Delft, The Netherlands, 2014.

37. Graham, M.; Allington-Jones, L. The Air-Abrasive Technique: A Re-Evaluation of Its Use in Fossil Preparation. *Palaeontol. Electron.* **2018**, 1–15. [CrossRef]